2025 IEEE/SICE International Symposium on System Integration (SII)
January 21-24, 2025, Munich, Germany

Comparative Study of Muscle Utilization in a Hybrid Controller Integrating Finite-State Impedance and Electromyography-Driven Musculoskeletal Model for Robotic Ankle Prostheses: A Case Study

M. Abdelbar[1], Atli Örn Sverrisson[2], Kristín Briem[3], Christophe Lecomte[2] and Sigurður Brynjólfsson[1]

Abstract— **The optimal neuroprosthetic control paradigm seeks to minimize the differences between artificial and natural physiology regarding subjective embodiment and dynamic performance. This study introduces a volitional control system integrating an electromyography (EMG)-driven musculoskeletal model with a finite state machine (FSM) impedance controller. A Hill-type muscle model is used to simulate the Gastrocnemius (GAS) and Tibialis Anterior (TA) muscles around the ankle joint. The system activates these muscles using input from ankle sensors and EMG data from antagonist muscles. To improve functionality and responsiveness, muscle parameters are optimized using a surrogate-based optimization approach. The impact of EMG control on a hybrid controller was analyzed, focusing on muscle activation during the stance phase. Two controllers were tested on a transtibial amputee for level-ground walking and stair ascent. Insights were gained into optimizing muscle activation for better gait dynamics. The model-based design technique was employed to automate validation, verification, and coding, reducing manual steps and errors. For level-ground walking, both hybrid controllers behaved more like an impedance controller than an EMG control. Disabling EMG control during plantarflexion with controller 1 prevented excessive plantarflexion, leading to a more natural gait. Controller 1, which used the TA muscle exclusively during controlled dorsiflexion, demonstrated greater repeatability. During stair ascent, both controllers allowed the user to place their toe first at each step, closely mimicking a natural gait pattern. Controller 2 exhibited better repeatability and slightly higher torque at the start of the controlled dorsiflexion phase, simplifying the control strategy and reducing computational effort.**

I. Introduction

People's quality of life is negatively impacted by lower limb amputation since it affects their ability to perform functional tasks [1], [2]. Passive prosthetics, which are incapable of restoring a significant portion of the joint's biological function, are prescribed to these individuals [3]. Powered prostheses are being developed to overcome this issue by aiming to be lightweight and produce torque and power comparable to those of an able-bodied joint [4-6].

These devices frequently use a finite state machine (FSM) controller, which divides the task into different states. When the user is in a state defined by the device, it usually provides torque or simulates impedance. These controllers are autonomous, which means that their control algorithm does not include any human input [7-11].

Electromyography (EMG) control has gained popularity recently as an approach to achieving lower limb prosthesis voluntary control [12], [13]. Incorporating human intent into these controllers enables amputees to voluntarily engage in varied activities and adjust their prosthetic mechanics to accommodate different terrains or unexpected obstacles. Moreover, Direct EMG control continually correlates the force generated with the muscle's signal [14]. This continuous volitional control allows individuals to do reactive and non-cyclic tasks by directly controlling and mimicking the biological musculoskeletal systems. Moreover, an EMG-driven musculoskeletal (MSK) model that is activated by the relative EMG signal magnitude of residual agonist-antagonist muscles can be used to achieve continuous volitional control (VC) of robotic ankle prostheses [15], [16].

However, amputees may experience increased mental and physical load if a control signal is continuously sent over long periods, potentially causing the user to become distracted or exhausted, which may result in a misinterpretation of the user's intentions and a decrease in performance and safety[17], [18]. Recently, control methods that benefit from the improved user control provided by VC control and the consistency and repeatability of non-VC control have been developed. Hybrid volitional control (HVC) integrates non-VC and VC methods that maintain non-VC stability and dependability while allowing the user to alter or enhance the limb's entire range of motion via VC. As a result, amputees can continually carry out a variety of basic tasks and modify the way their devices move to carry out tasks that are currently difficult for them [19], [20].

Moreover, the model-based design (MBD) technique is used to improve the control of robotic systems. By applying models systematically throughout the development process, MBD is an approach that optimizes the delivery of complex systems [21]. MBD automates many stages of the software development process, including testing and code generation, which dramatically reduces the amount of time required to construct complicated systems. Tony Shu et al. utilized model-based design (MBD) to develop direct myoelectric control of a subject-optimized neuromuscular model [22].

In this paper, a VC based on an EMG-driven MSK model was integrated with an FSM impedance controller. A Hill-type muscle model was employed to simulate the functions of the Gastrocnemius (GAS) and Tibialis Anterior (TA) muscles around the ankle joint. To activate these muscle models, the system utilizes input from ankle sensors and EMG data from the antagonist muscle pair. Furthermore, to improve the

This research was funded by the Technology Development Fund at the Icelandic Center for Research (grant no. 2215370-0611).

[1]Faculty of Industrial Engineering, Mechanical Engineering and Computer Science, University of Iceland, 107 Reykjavík, Iceland (e-mails: msm18@hi.is, sb@hi.is).

[2]Össur hf., Grjóthals 5, 110 Reykjavik, Iceland (e-mail: clecomte@ossur.com).

[3]School of Health Sciences, University of Iceland, 101 Reykjavík, Iceland (e-mail: kbriem@hi.is).

functionality and responsiveness of the neuromuscular model controller, muscle parameters within the model are optimized using a surrogate-based optimization (SBO) approach. This paper also investigates the effects of using EMG control to examine and compare the impact of activating different muscles within the context of a neuromuscular model during the stance phase on a hybrid controller. The study involved testing two different controllers on a transtibial amputee (TTA) user during level-ground walking and stair ascent, providing new insights into optimizing muscle activation for improved gait dynamics. Moreover, the MBD technique developed the controller to decrease manual steps and human errors by automating essential steps like validation, verification, and coding.

II. Methods

A. Finite-State Machine Impedance Controller

The four states of the finite-state machine (FSM) in use are powered pushing (PP), controlled dorsiflexion (CD), controlled plantarflexion (CP), and swing (SW). The torque is stated as follows in each:

$$\tau_{FSM} = k_n(\theta - \theta_n^*) + b_n\dot{\theta} \quad (1)$$

Where the ankle angle and angular velocity are represented by θ and $\dot{\theta}$, while representing the linear stiffness, damping coefficient, and equilibrium point of the n-th state are represented by k_n, b_n, and θ_n^*, respectively [20], [23]. The initial impedance control parameters are shown for each state in Table I. These can be changed if needed to meet the user's comfort or other needs.

Moreover, the FSM transitions directly into CD if the user does not plantarflex during initial contact during stair ascent. This adaptation enhances movement and stability by allowing the controller to prioritize dorsiflexion, which is necessary for lifting the foot and clearing the stairs.

TABLE I. Initial Impedance Control Parameters

State	*CP*	*CD*	*PP*	*SW*
$k_n\ (Nm/deg)$	1	2	5	2
$b_n\ (Nms/deg)$	0.02	0.005	0	0
$\theta_n^*\ (deg)$	0	0	-10	0

B. Surface Electromyography Signal Acquisition and Analysis

The surface EMG signals of the participant's TA and GAS muscles were recorded using Össur's prosthetic assembly, which includes an electrode interface for measuring muscle activity. This interface consists of a dome electrode attached to the prosthetic liner and an electrical conduit that transmits the electrical potential from the user's skin surface to the outside of the liner, ultimately connecting to the prosthetic socket. [24].

Surface EMG signals were prefiltered in the amplifier using a 20 Hz high-pass filter and a 50 Hz notch filter to remove power grid noise. The signals were then sampled at 1000 Hz. The signal was rectified and smoothed with a 2 Hz low-pass Butterworth filter to create a linear envelope, which was normalized to the user's maximal voluntary contraction (MVC) for control signal generation. Additionally, an adaptive moving average filter was applied to remove artifacts which Össur designed [24].

Furthermore, depending just on the normalized muscle activation signal is insufficient due to the time-varying nature of the EMG signal, especially in dynamic circumstances [25]. As a result, the activation dynamic model used in [25] was applied to the system.

C. Neuromuscular Model

The construction of a neuromuscular (NM) model is based on the dynamics of muscle contraction and musculoskeletal geometry. The equations for contraction dynamics transform the levels of muscle activation into the corresponding muscle forces. This involves understanding the force-length and force-velocity properties of muscles, as well as activation and deactivation kinetics. The Hill-type model was used to simulate the contraction dynamics of the muscle-tendon unit (MTU). The integration of musculoskeletal geometry involves the modeling of the anatomical structure, including joint angles, moment arms, and muscle attachments, to precisely depict the transmission of forces and production of movement in the body. Together, these components enable the NM model to simulate realistic muscle behavior and movement as it is implemented [26-30].

D. Model-Based Design of Neuromuscular Model

The MBD process is shown in Fig.1. It starts by collecting and formalizing requirements, and then goes on to modeling and automatic code generation. It is important to guarantee two-way traceability between all development artifacts, including requirements, models, code, and test cases.

Testing is performed at every stage of the development process: code that is run on a PC or the target is tested against the model, and the model is tested against the requirements [31].

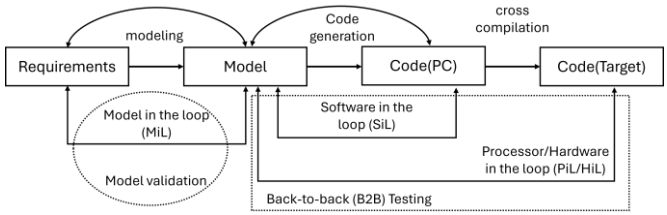

Figure 1. MBD Workflow [30].

1) Modeling of the Neuromuscular Model

The model has been designed to reflect the system as precisely as possible and to ensure that the controller used in the model encounters the same challenges and conditions as the real model to reduce modeling errors. Furthermore, the Infinite-Impulse-Response (IIR) discrete filter was used to represent the discrete version of the second-order differential equation of the activation dynamics model stated in Section II-B, and integration of discrete-time is done by applying the Forward Euler Integration Method. The NM controller's dynamic model implementation using MATLAB -Simulink [32] is shown in Fig. 2.

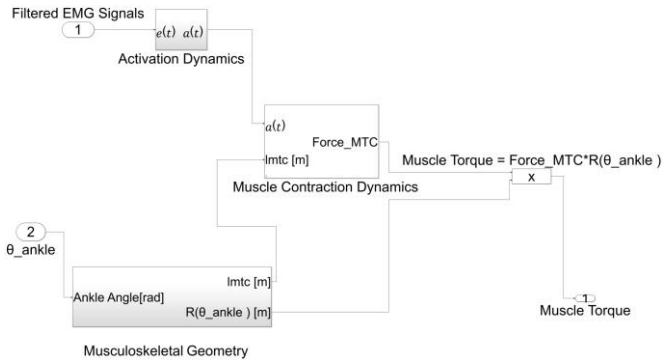

Figure 2. The dynamic model of the Neuromuscular model controller.

The system was optimized using a surrogate-based optimization approach [33], with the squared error between biological ankle torque and model-predicted ankle torque defined as the cost function [34]. The dataset introduced by Camargo et al. [35] is used in this research to solve the optimization problem.

2) Automated Code Generation and Validation of the Neuromuscular Model

Furthermore, the optimized MATLAB-Simulink NM model controller was exported as a C++ library for controller implementation to create the NM controller software using the MATLAB Coder extension [36]. A software-in-the-loop (SIL) simulation has also been performed to validate and verify the system. This involves making sure that embedded software, control loops, and algorithms function as intended. Then, a processor-in-the-loop (PIL) simulation is performed to ensure that the hardware can execute the controller software without unexpected problems and that the outputs match what was expected. The verified NM controller software is then integrated with the FSM impedance controller and the rest of the system.

E. Hybrid FSM Impedance and EMG-Driven MSK Model Controller

During the stance phase, a hybrid FSM impedance and EMG-driven MSK model controller is used. Where the total torque (τ_t) is equal to the torque of the NM controller (τ_m) in addition to the FSM impedance controller torque (τ_{FSM}).

$$\tau_t(t) = \tau_m(t) + \tau_{FSM}(t) \quad (2)$$

The ankle behavior during the swing phase can be represented as a position control of the ankle joint around the state, as defined in [37], by setting the ankle equilibrium point θ_n^* and the damping coefficient b_n to zero as indicated in Table I. The controller operates in hybrid mode until it validates that the foot is entirely off the ground to ensure a smooth transition to the swing phase of the gait. An ankle angle controls the change from hybrid to position control. The hybrid FSM impedance and EMG-driven musculoskeletal model controller's block diagram is shown in Fig. 3.

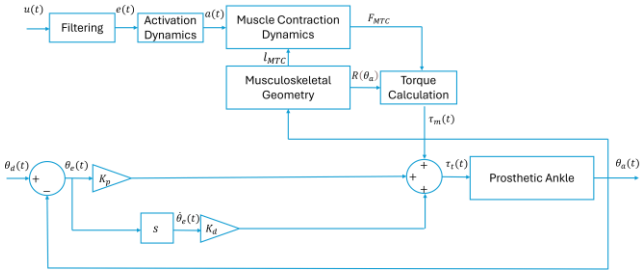

Figure 3. Block diagram of the hybrid FSM impedance and EMG-driven musculoskeletal model controller.

F. Muscle Utilization in Controller Design

1) Controller 1

For controller 1, the NM torque $\tau_m(t)$ is calculated as the difference between the torque from the TA muscle τ_{m-TA} and the GAS muscle τ_{m-GAS} during the stance phase. Using both muscles during the controlled plantarflexion (CP) and controlled dorsiflexion (CD) phases ensures smoother transitions and better stability, especially for users with low muscle co-contraction. This aids in balance and provides a more natural gait pattern.

$$\tau_m = \tau_{m-TA} - \tau_{m-GAS} \quad (1)$$

However, the negative torque of the gastrocnemius muscle $-\tau_{m-GAS}$ represents the NM torque only during the PP phase. GAS is the principal muscle engaged in plantarflexion, which is important to effectively raising the foot off the ground and generating forward motion. The control system may depend solely on the GAS muscle to optimize torque to provide an explosive and efficient push-off. Controlling opposing forces from the tibialis anterior (TA) muscle reduces computational complexity and simplifies the control approach because the TA muscle is not as active during this period. Table II provides an overview of the muscles used in the stance phase to calculate the $\tau_m(t)$ for controller 1.

TABLE II. ESTIMATION OF τ_m FOR NM CONTROLLER FOR CONTROLLER 1 THROUGHOUT THE STANCE PHASE.

Subphase	***NM CONTROLLER***
CP	$\tau_m = \tau_{m-TA} - \tau_{m-GAS}$
CD	$\tau_m = \tau_{m-TA} - \tau_{m-GAS}$
PP	$\tau_m = -\tau_{m-GAS}$

2) Controller 2

To avoid excessive forces and instability during the CP phase, the controller avoids applying excess plantarflexion torque. For some users, integrating the impedance controller with NM torque during this phase may result in excessive torque. Therefore, the controller disables the NM model and relies solely on the impedance controller during CP for a smoother transition into CD.

Furthermore, the second controller was designed to use only the TA muscle during the CD phase. This simplifies the control strategy and reduces computational effort. Using the TA muscle helps the tibia rollover and increases dorsiflexion torque in CD, leading to less foot stiffness, which is advantageous for activities like stair ascent. This approach also benefits users with high muscle co-contraction by

providing better control and stability during the CD phase.

Additionally, using both muscles risks over-activation, potentially leading to muscle fatigue, and it may avoid the risk of high co-contractions. Table III provides an overview of the muscles used in the stance phase to calculate the $\tau_m(t)$ for controller 2.

TABLE III. ESTIMATION OF τ_m FOR NM CONTROLLER FOR CONTROLLER 2 THROUGHOUT THE STANCE PHASE.

Subphase	*NM CONTROLLER*
CP	$\tau_m = 0$
CD	$\tau_m = \tau_{m-TA}$
PP	$\tau_m = -\tau_{m-GAS}$

III. EXPERIMENTAL SETUP AND RESULTS

The user testing protocol CII2019061252 has been approved by the Icelandic National Bioethics Committee (VSN-19-083-V42). There was only one user. The participant gave written informed consent to participate in the study. The participant in the study is a 56-year-old male, standing 179 cm tall and weighing 103 kg. He has been living with an amputation for 19 years, which resulted from trauma. The amputation is on his right side, and he currently uses an Össur Pro-Flex Pivot prosthetic daily. Two tasks were employed to assess the performance of the two controllers: level-ground walking and stair ascent.

The user walked on level ground at a pace of at an average speed of 1 m/s by applying controller 1 and controller 2 as described in Section II-F. The EMG activity of the GAS and TA muscles, ankle angle, ankle total torque, and NM torque during level-ground walking testing are shown respectively in Figs. 4 to 8. Each figure displays the outputs from both controllers, providing a comparative view of their performance across these variables.

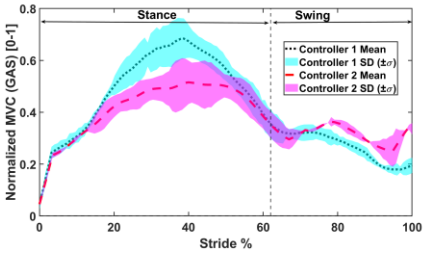

Figure 4. EMG activity for the GAS muscle averaged over strides ±1 standard deviation (shading) during the level-ground walking testing.

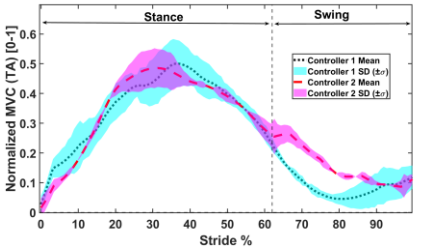

Figure 5. EMG activity for the TA muscle averaged over strides ±1 standard deviation (shading) during the level-ground walking testing.

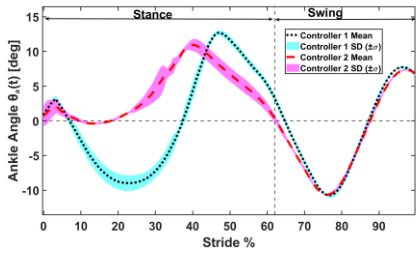

Figure 6. Ankle angle $\theta_a(t)$ averaged over strides ±1 SD shading (positive for dorsiflexion, negative for plantarflexion) during level-ground walking.

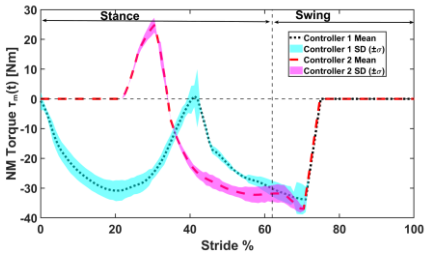

Figure 7. Ankle NM torque $\tau_m(t)$ averaged over strides ±1 SD shading (positive for dorsiflexion, negative for plantarflexion) during level-ground walking.

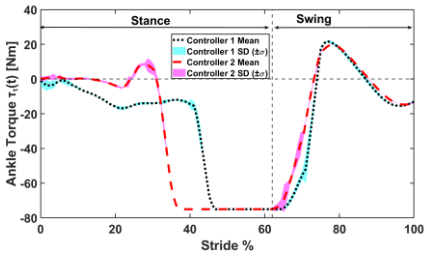

Figure 8. Ankle total torque $\boldsymbol{\tau_t(t)}$ averaged over strides ±1 SD shading (positive for dorsiflexion, negative for plantarflexion) during level-ground walking.

Furthermore, the user ascended stairs using controller 1 and controller 2, as outlined in Section II-F. Figs. 9 to 13 illustrate the EMG activity of the GAS and TA muscles, ankle angle, ankle total torque, and NM torque during stair ascent. Each figure presents the results from both controllers, allowing for a comparative analysis of their performance across these outputs.

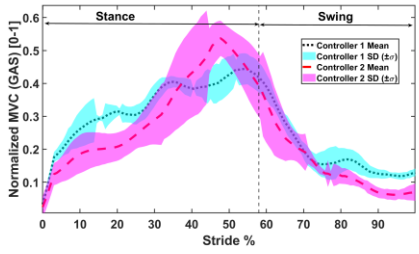

Figure 9. EMG activity for the GAS muscle averaged over strides ±1 standard deviation (shading) during the stair ascent testing.

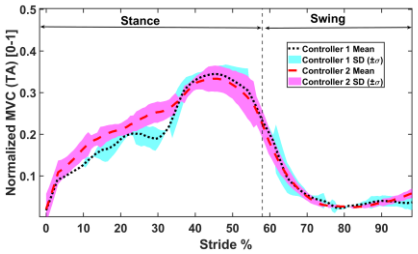

Figure 10. EMG activity for the TA muscle averaged over strides ±1 standard deviation (shading) during the stair ascent testing.

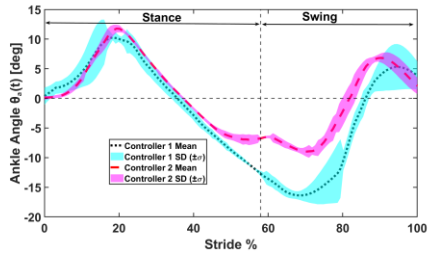

Figure 11. Ankle angle $\theta_a(t)$ averaged over strides ±1 SD shading (positive for dorsiflexion, negative for plantarflexion) during stair ascent.

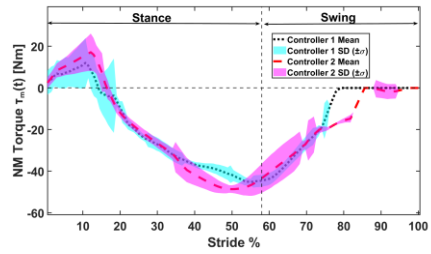

Figure 12. Ankle NM torque $\tau_m(t)$ averaged over strides ±1 SD shading (positive for dorsiflexion, negative for plantarflexion) during stair ascent.

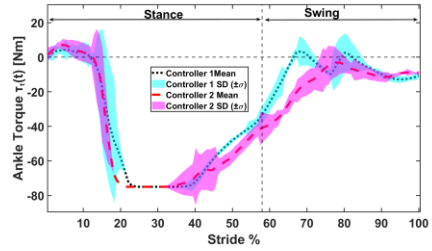

Figure 13. Ankle total torque $\tau_t(t)$ averaged over strides ±1 SD shading (positive for dorsiflexion, negative for plantarflexion) during stair ascent.

IV. DISCUSSION AND CONCLUSIONS

A. *Level-Ground Walking*

Fig. 7 shows that NM torque, influenced by muscle activity and ankle angle inputs, caused Controller 1 to have high torque during the controlled plantarflexion (CP) phase, leading to increased ankle plantarflexion (Fig. 6). High torque and ankle angle during this phase can cause excessive plantarflexion, which affects stability and smooth movement. Disabling NM during the CP phase for Controller 2 can avoid excessive torque, resulting in a more natural gait cycle.

Moreover, the PP phase was initiated earlier due to the ankle angle and the additional dorsiflexion torque provided by the NM controller in controller 2. As shown in Fig. 8, the peak torque, which represents the maximum torque that can be applied to the ankle 75 N·m, started earlier with controller 2. However, the standard deviation data indicate that controller 1 demonstrated greater repeatability.

A review of the torque data and user feedback indicates that the impedance controller has a stronger effect than the neuromuscular (NM) control. Consequently, the overall behavior of both controllers aligns more closely with that of an impedance controller.

B. *Stair Ascent*

Disabling the NM torque during the controlled CP phase did not impact the stair ascent results because the user effectively bypassed this phase. The user skips loading the heel at initial contact during stair ascent, transitioning directly into CD.

Both controllers enabled the user to place their toe first at the beginning of each step, closely replicating a natural gait pattern. The EMG controller adjusted torque in response to muscle activity (Fig. 12), facilitating smooth and natural movement. It provided additional propulsion during the PP phase, which was essential for generating the force needed to lift the body onto the next step (Fig. 13).

During the stance phase, there was no significant difference between Controller 1 and Controller 2. However, Controller 2 demonstrated better repeatability and slightly higher torque at the beginning of the CD phase due to the exclusive use of the TA muscle (Fig. 11), which makes the ankle less stiff during the CD phase. Controller 2 simplifies the control strategy by focusing on a single muscle, which reduces the overall complexity of the controller and lowers the computational effort required for real-time processing.

The transition to the swing phase took longer during stair ascent compared to level-ground walking due to the increased biomechanical demands of ascending stairs. This is because the PP phase requires additional time to ensure that the entire foot is completely off the ground and because the foot must be lifted higher during the swing phase to clear the step.

The positive outcomes from these results encourage future research initiatives. More users with transtibial amputations will test the hybrid controller during daily functional activities, and additional biomechanical testing will be conducted to evaluate its effectiveness.

REFERENCES

[1] K. E. Zelik, K. Z. Takahashi, and G. S. Sawicki, "Six degree-of-freedom analysis of hip, knee, ankle and foot provides updated understanding of biomechanical work during human walking," Journal of Experimental Biology, vol. 218, no. 6, pp. 876–886, Mar. 2015, doi: 10.1242/jeb.115451.

[2] J. R. Usherwood, A. J. Channon, J. P. Myatt, J. W. Rankin, and T. Y. Hubel, "The human foot and heel-sole-toe walking strategy: A mechanism enabling an inverted pendular gait with low isometric muscle force?," J R Soc Interface, vol. 9, no. 75, pp. 2396–2402, Oct. 2012, doi: 10.1098/rsif.2012.0179.

[3] M. Goldfarb, "Consideration of Powered Prosthetic Components as They Relate to Microprocessor Knee Systems," JPO Journal of

Prosthetics and Orthotics, vol. 25, no. 4S, pp. P65-P75, Oct. 2013, doi: 10.1097/JPO.0b013e3182a8953e.

[4] H. Houdijk, E. Pollmann, M. Groenewold, H. Wiggerts, and W. Polomski, "The energy cost for the step-to-step transition in amputee walking," Gait Posture, vol. 30, no. 1, pp. 35–40, Jul. 2009, doi: 10.1016/j.gaitpost.2009.02.009.

[5] H. M. Herr and A. M. Grabowski, "Bionic ankle-foot prosthesis normalizes walking gait for persons with leg amputation," Proceedings of the Royal Society B: Biological Sciences, vol. 279, no. 1728, pp. 457–464, 2012, doi: 10.1098/rspb.2011.1194.

[6] S. Lipfert, M. Günther, D. Renjewski, and A. Seyfarth, "Erratum: Impulsive ankle push-off powers leg swing in human walking (Journal of Experimental Biology 217 (1218-1228))," May 15, 2014, Company of Biologists Ltd. doi: 10.1242/jeb.107391.

[7] F. Sup, A. Bohara and M. Goldfarb, "Design and Control of a Powered Knee and Ankle Prosthesis," Proceedings 2007 IEEE International Conference on Robotics and Automation, Rome, Italy, 2007, pp. 4134-4139, doi: 10.1109/ROBOT.2007.364114.

[8] M. Liu, F. Zhang, P. Datseris, and H. (Helen) Huang, "Improving Finite State Impedance Control of Active-Transfemoral Prosthesis Using Dempster-Shafer Based State Transition Rules," Journal of Intelligent and Robotic Systems: Theory and Applications, vol. 76, no. 3–4, pp. 461–474, Oct. 2014, doi: 10.1007/s10846-013-9979-3.

[9] T. Best et al., "Phase-Based Impedance Control of a Powered Knee-Ankle Prosthesis for Tuning-Free Locomotion over Speeds and Inclines," 2020, doi: 10.36227/techrxiv.19165895.v4.

[10] S. Au, M. Berniker, and H. Herr, "Powered ankle-foot prosthesis to assist level-ground and stair-descent gaits," Neural Networks, vol. 21, no. 4, pp. 654–666, May 2008, doi: 10.1016/j.neunet.2008.03.006.

[11] S. Culver, H. Bartlett, A. Shultz, and M. Goldfarb, "A stair ascent and descent controller for a powered ankle prosthesis," IEEE Transactions on Neural Systems and Rehabilitation Engineering, vol. 26, no. 5, pp. 993–1002, May 2018, doi: 10.1109/TNSRE.2018.2819508.

[12] B. Ahkami, K. Ahmed, A. Thesleff, L. Hargrove, and M. Ortiz-Catalan, "Electromyography-Based Control of Lower Limb Prostheses: A Systematic Review," IEEE Trans Med Robot Bionics, vol. 5, no. 3, pp. 547–562, Aug. 2023, doi: 10.1109/TMRB.2023.3282325.

[13] A. Fleming et al., "Myoelectric control of robotic lower limb prostheses: A review of electromyography interfaces, control paradigms, challenges and future directions," Aug. 01, 2021, IOP Publishing Ltd. doi: 10.1088/1741-2552/ac1176.

[14] K. G. Rabe, T. Lenzi, and N. P. Fey, "Performance of Sonomyographic and Electromyographic Sensing for Continuous Estimation of Joint Torque during Ambulation on Multiple Terrains," IEEE Transactions on Neural Systems and Rehabilitation Engineering, vol. 29, pp. 2635–2644, 2021, doi: 10.1109/TNSRE.2021.3134189.

[15] D. L. Crouch and H. Huang, "Lumped-parameter electromyogram-driven musculoskeletal hand model: A potential platform for real-time prosthesis control," J Biomech, vol. 49, no. 16, pp. 3901–3907, Dec. 2016, doi: 10.1016/j.jbiomech.2016.10.035.

[16] L. Pan, D. L. Crouch, and H. Huang, "Myoelectric Control Based on a Generic Musculoskeletal Model: Toward a Multi-User Neural-Machine Interface," IEEE Transactions on Neural Systems and Rehabilitation Engineering, vol. 26, no. 7, pp. 1435–1442, Jul. 2018, doi: 10.1109/TNSRE.2018.2838448.

[17] L. Hargrove, "Volitional control research," in Full Stride: Advancing the State of the Art in Lower Extremity Gait Systems, Springer New York, 2017, pp. 137–150. doi: 10.1007/978-1-4939-7247-0_8.

[18] O. Bai et al., "A wireless, smart EEG system for volitional control of lower-limb prosthesis," TENCON 2015 - 2015 IEEE Region 10 Conference, Macao, China, 2015, pp. 1-6, doi: 10.1109/TENCON.2015.7373060.

[19] B. Chen, Q. Wang, and L. Wang, "Adaptive Slope Walking with a Robotic Transtibial Prosthesis," IEEE/ASME Trans. Mechatronics, vol. 20, no. 5, pp. 2146–2157, Oct. 2015, doi: 10.1109/TMECH.2014.2365877.

[20] R. R. Posh, J. P. Schmiedeler, and P. M. Wensing, "Finite-State Impedance and Direct Myoelectric Control for Robotic Ankle Prostheses: Comparing Their Performance and Exploring Their Combination," IEEE Transactions on Neural Systems and Rehabilitation Engineering, vol. 31, pp. 2778–2788, 2023, doi: 10.1109/TNSRE.2023.3287971.

[21] G. Barbieri, C. Fantuzzi, and R. Borsari, "A model-based design methodology for the development of mechatronic systems," Mechatronics, vol. 24, no. 7, pp. 833–843, Oct. 2014, doi: 10.1016/j.mechatronics.2013.12.004.

[22] T. Shu et al., "Modulation of Prosthetic Ankle Plantarflexion Through Direct Myoelectric Control of a Subject-Optimized Neuromuscular Model," IEEE Robot Autom Lett, vol. 7, no. 3, pp. 7620–7627, Jul. 2022, doi: 10.1109/LRA.2022.3183762.

[23] F. J. Abu-Dakka and M. Saveriano, "Variable Impedance Control and Learning—A Review," Dec. 21, 2020, Frontiers Media S.A. doi: 10.3389/frobt.2020.590681.

[24] Atli Örn Sverrisson and Jóna Sigrún Sigurðardóttir, "Prosthetic assembly having an electrode interface for recording muscle activity," U.S. Patent WO2023064323A1, 20, Apr 2023.

[25] Buchanan TS, Lloyd DG, Manal K, Besier TF. Neuromusculoskeletal modeling: estimation of muscle forces and joint moments and movements from measurements of neural command. J Appl Biomech. 2004 Nov;20(4):367-95. doi: 10.1123/jab.20.4.367. PMID: 16467928; PMCID: PMC1357215.

[26] M. F. Eilenberg, H. Geyer, and H. Herr, "Control of a powered ankle-foot prosthesis based on a neuromuscular model," IEEE Transactions on Neural Systems and Rehabilitation Engineering, vol. 18, no. 2, pp. 164–173, Apr. 2010, doi: 10.1109/TNSRE.2009.2039620.

[27] H. Geyer and H. Herr, "A Muscle-reflex model that encodes principles of legged mechanics produces human walking dynamics and muscle activities," IEEE Transactions on Neural Systems and Rehabilitation Engineering, vol. 18, no. 3, pp. 263–273, Jun. 2010, doi: 10.1109/TNSRE.2010.2047592.

[28] H. Geyer and A. Seyfarth, "Neuromuscular Control Models of Human Locomotion," in Humanoid Robotics: A Reference, P. Vadakkepat and A. Goswami, Eds., Springer Dordrecht, 2019. doi: 10.1007/978-94-007-7194-9_45-1.

[29] H. Geyer, A. Seyfarth, and R. Blickhan, "Positive force feedback in bouncing gaits?," Proceedings of the Royal Society B: Biological Sciences, vol. 270, no. 1529, pp. 2173–2183, Oct. 2003, doi: 10.1098/rspb.2003.2454.

[30] M. Abdelbar, A. Örn Sverrisson, K. Briem, C. Lecomte and S. Brynjólfsson, "A Hybrid Controller Integrating Finite-State Impedance and Electromyography-Driven Musculoskeletal Model for Robotic Active Ankle Prostheses: A Case Study," in *IEEE Access*, vol. 12, pp. 157329-157345, 2024, doi: 10.1109/ACCESS.2024.3485570.

[31] J. Babić, S. Marijan, and I. Petrović, "Model-Based Techniques for Real-Time Embedded Applications," Automatika, vol. 52, no. 4, pp. 329–338, Jan. 2011, doi: 10.1080/00051144.2011.11828432.

[32] The MathWorks Inc., "MATLAB version: 23.2.0 (R2023b)," Natick, Massachusetts, 2023. Available: https://www.mathworks.com.

[33] M. Abdelbar et al., "Optimization of PI-Cascaded Controller's Parameters for Linear Servo Mechanism: A Comparative Study of Multiple Algorithms," IEEE Access, vol. 11, pp. 86377–86396, 2023, doi: 10.1109/ACCESS.2023.3304333.

[34] C. Shah, A. Fleming, V. Nalam, M. Liu, and H. H. Huang, "Design of EMG-driven Musculoskeletal Model for Volitional Control of a Robotic Ankle Prosthesis," in IEEE International Conference on Intelligent Robots and Systems, Institute of Electrical and Electronics Engineers Inc., 2022, pp. 12261–12266. doi: 10.1109/IROS47612.2022.9981305.

[35] J. Camargo, A. Ramanathan, W. Flanagan, and A. Young, "A comprehensive, open-source dataset of lower limb biomechanics in multiple conditions of stairs, ramps, and level-ground ambulation and transitions," J Biomech, vol. 119, Apr. 2021, doi: 10.1016/j.jbiomech.2021.110320.

[36] The MathWorks Inc., "Embedded Coder version: 23.2.0 (R2023b)," Natick, Massachusetts, 2023. Available: https://www.mathworks.com.

[37] M. Eilenberg, "A Neuromuscular-Model Based Control Strategy for Powered Ankle-Foot Prostheses," M.S. thesis, Mechanical Engineering, Massachusetts Institute of Technology, Cambridge, Massachusetts, USA, 2009.